MAGNETOHYDRODYNAMICS Vol. 42 (2006), No. 2–3, pp. 153–160

EXPERIMENTAL ASPECTS OF CONTACTLESS INDUCTIVE FLOW TOMOGRAPHY

Th. Gundrum, G. Gerbeth, F. Stefani, M. Xu

Forschungszentrum Rossendorf, P.O. Box 510119, D-01314 Dresden, Germany

Contactless inductive flow tomography (CIFT) is aimed at velocity reconstruction in electrically conducting melts, which are used in many metallurgical and crystal growth applications. Under the influence of an externally applied magnetic field the flow induced current produces a perturbation of the applied field, which can be measured outside the fluid volume. The alternating application of two orthogonal external fields represents a minimum for the detection of both poloidal and toroidal velocity components. The paper gives an introduction to CIFT and describes its first experimental application to a propeller driven flow of the liquid alloy GaInSn.

Introduction. In silicon crystal growth, in continuous casting of steel and many other industrial processes, there is an urgent need for a non-invasive, contactless determination of the three-dimensional flow field of the melt. Evidently, the established optical flow measurement techniques do not work in those opaque fluids. But even Ultrasonic Doppler Velocimetry (UDV) is not always applicable when it comes to measurement tasks in very hot and/or chemically aggressive fluids. It should be noticed that in many applications even the knowledge of the rough flow structure would be valuable.

Fortunately, the concerned metallic and semiconducting melts are characterized by a relatively high electrical conductivity. When exposed to an externally applied magnetic field, the melt flow produces electric currents, which give rise to a perturbation of the applied field. This flow induced field perturbation, which is detectable outside the fluid volume, carries information about the flow structure and can be exploited to reconstruct the velocity field.

Such a velocity reconstruction has much in common with magnetoencephalography [1], which aims at inferring neuronal activity in the brain from external magnetic field measurements. In contrast to magnetoencephalography, the sought-for velocity field can be exposed to *different* external magnetic fields, and all the different resulting field perturbations can be utilized to gain detailed information about the velocity field. Another, more technical difference to magnetoencephalography concerns the magnitude of the measured magnetic fields (μT instead of fT or pT), which allows the application of much cheaper Hall sensors instead of SQUIDs. In this paper, we report on a first experimental demonstration of such a *contactless inductive flow tomography* (CIFT) and its validation by UDV measurements.

1. Theory. Assume a liquid with an electrical conductivity σ and a magnetic permeability μ, flowing with a typical velocity v in a volume characterized by the linear dimension l. Then the ratio of the flow induced magnetic field to the externally applied magnetic field is governed by the magnetic Reynolds number, $\mathrm{Rm} = \mu\sigma v l$. In many technical and experimental flows of liquid metals and semiconducting melts, Rm is of the order of 0.01...1. Only in very special applications (fast breeder reactors, dynamo experiments), Rm acquires values much greater than 1.

Suppose now the velocity field $\mathbf{v}(\mathbf{r})$ to be stationary, and the melt to be exposed to an externally applied magnetic field $\mathbf{B}_0$. According to Ohm's law in moving conductors, we get a current

$$\mathbf{j} = \sigma(\mathbf{v} \times \mathbf{B}_0 - \nabla\varphi) \,, \tag{1}$$

with φ denoting the electric potential. This current, in turn, induces an additional magnetic field $\mathbf{b}$ with

$$\begin{aligned} \mathbf{b}(\mathbf{r}) &= \frac{\mu_0\sigma}{4\pi} \int_V \frac{(\mathbf{v}(\mathbf{r}') \times \mathbf{B}_0(\mathbf{r}')) \times (\mathbf{r} - \mathbf{r}')}{|\mathbf{r} - \mathbf{r}'|^3} \, \mathrm{d}V' \\ &\quad - \frac{\mu_0\sigma}{4\pi} \int_S \varphi(\mathbf{s}')\mathbf{n}(\mathbf{s}') \times \frac{\mathbf{r} - \mathbf{s}'}{|\mathbf{r} - \mathbf{s}'|^3} \, \mathrm{d}S' \,. \end{aligned} \tag{2}$$

Equation (2) follows from substituting Eq. (1) for the current $\mathbf{j}$ into the Biot–Savart law and transforming the volume integral over $\nabla\varphi$ into a surface integral over φ. Strictly speaking, the applied field $\mathbf{B}_0$ under the integral in Eq. (2) must be replaced by the total field $\mathbf{B} = \mathbf{B}_0 + \mathbf{b}$, but as long as Rm is small, the induced field $\mathbf{b}$ can be neglected at this position.

The electric potential φ at the boundary S, which appears in Eq. (2), has to fulfill the boundary integral equation

$$\begin{aligned} \varphi(\mathbf{s}) &= \frac{1}{2\pi} \int_D \frac{(\mathbf{v}(\mathbf{r}') \times \mathbf{B}_0(\mathbf{r}')) \cdot (\mathbf{s} - \mathbf{r}')}{|\mathbf{s} - \mathbf{r}'|^3} \, \mathrm{d}V' \\ &\quad - \frac{1}{2\pi} \int_S \varphi(\mathbf{s}')\mathbf{n}(\mathbf{s}') \cdot \frac{\mathbf{s} - \mathbf{s}'}{|\mathbf{s} - \mathbf{s}'|^3} \, \mathrm{d}S' \,, \end{aligned} \tag{3}$$

which follows from taking in Eq. (1) the divergence of the current and utilizing $\nabla \cdot \mathbf{j} = 0$. Then, the Green's theorem can be applied to the solution of the arising Poisson equation $\Delta\varphi = \nabla \cdot (\mathbf{v} \times \mathbf{B})$, with demanding that the current is purely tangential at the boundary [3]. Actually, Eq. (3) is at the root of the vast area of *electric* inductive flow measurements [4] which is, however, not the subject of the present work.

In the first instance, Eqs. (2) and (3) are a recipe to compute the induced magnetic field $\mathbf{b}$ and the induced electric potential φ for a given velocity field $\mathbf{v}$ (this remains true in the dynamo relevant case of large Rm, where $\mathbf{B}_0$ under the integrals must be replaced by $\mathbf{B}$: then we have to solve an integral equation system instead of computing only the integrals [5]). However, they also allow to infer the velocity field if the induced (electro-)magnetic fields are given. This represents a typical inverse problem with intricate uniqueness questions.

It was the main result of the paper [6] that the velocity field could be reconstructed from the external measurement of an appropriate component of the induced magnetic field (e.g., the radial component for a spherically shaped fluid volume) *and* the electric potential at the fluid boundary apart from an uncertainty in the radial distribution of the flow.

Based on this result, in [7] we have proposed a general method how the electric potential measurement at the fluid boundary can be avoided. The main idea is to apply the external magnetic field in two different, e.g., orthogonal, directions and to measure both corresponding sets of induced magnetic fields. For this, it is needed to treat the electric potential at the boundary in an implicit way. The remaining non-uniqueness is "solved" by means of Tikhonov regularization, by which we obtain a velocity solution that represents a reasonable compromise

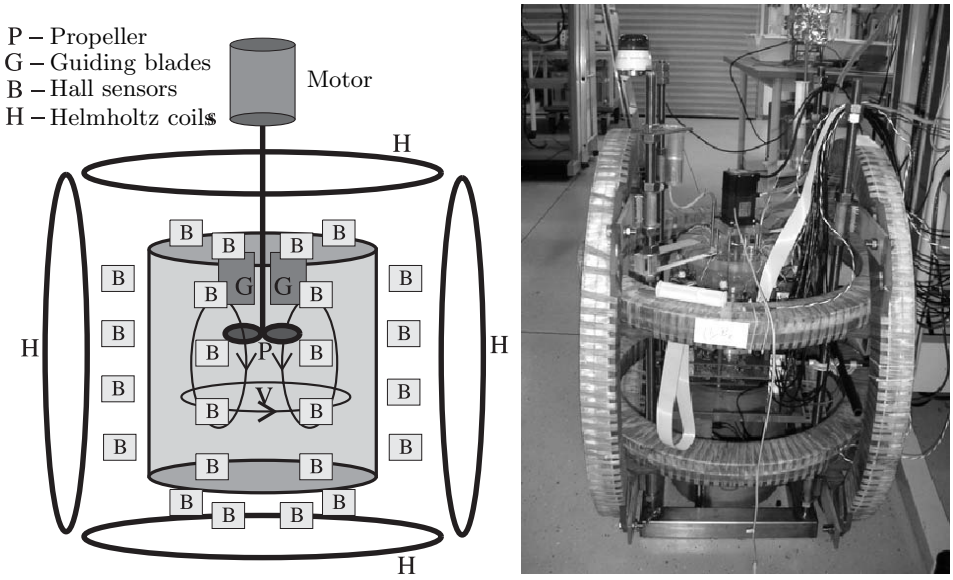

(*a*) (*b*)

Fig. 1. The set-up of the CIFT experiment. (*a*) Principle scheme. (*b*) Photograph.

between fitting the measured data and having not too large kinetic energy. The mathematical details on how to solve the inverse problem of CIFT can be found in [2, 7, 8]. In the following, we will focus on the experimental problems.

2. Experiment. In order to validate the theory of CIFT in laboratory, we have set up a demonstration experiment (Fig. 1). A polypropylene vessel with an inner diameter of 18.0 cm is filled with 4.4 liters of the eutectic alloy $Ga^{67}In^{20.5}Sn^{12.5}$ (which is liquid at room temperatures) up to a hight of 17.2 cm. The flow is produced by a motor driven propeller with a diameter of 6 cm. The propeller is positioned approximately at one third of the total hight measured from the top (Fig. 2*a*). Eight guiding blades above the propeller are intended to remove

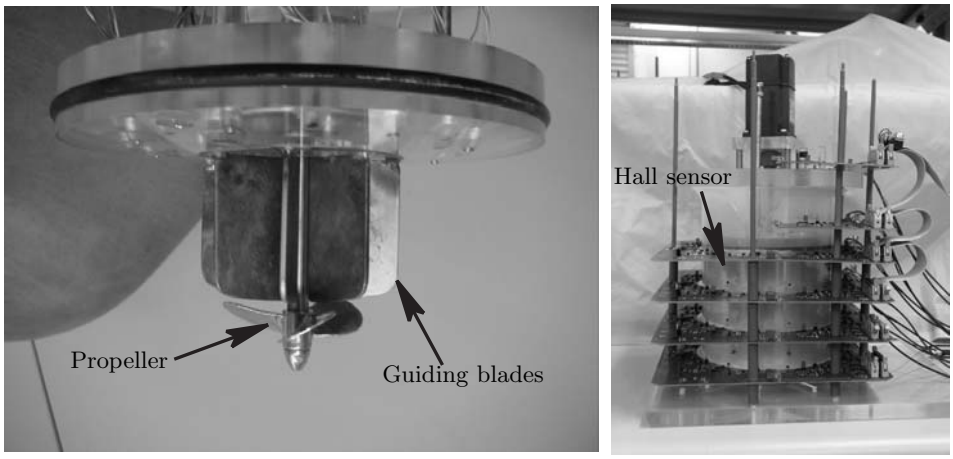

(*a*) (*b*)

Fig. 2. (*a*) Propeller and guiding blades close to the top lid of the vessel. (*b*) The vessel with a part of the circuit boards carrying 48 Hall sensors and Signal conditioning.

the swirl of the flow in case that the propeller pumps upwards. In contrast to that, the downward pumping produces, in addition to the main poloidal motion, a considerable toroidal motion. The rotation rate of the propeller can reach up to 2000 rpm that amounts to a mean velocity of approximately 1 m/s, corresponding to a magnetic Reynolds number of approximately 0.4.

The induced magnetic fields are measured by 48 external Hall sensors, 8 of them grouped together on 6 circuit boards, which are located at different heights (Fig. 2*b*). Partly, a 49th sensor has been used, which was positioned in the center below the vessel.

The axial and the transversal fields of about 5 mT are alternately produced by two pairs of Helmholtz coils, which are fed by currents of 22.5 A and 32.5 A, respectively. Both fields are applied for a period of 3 s, during which a trapezoidal signal form is imposed (Fig. 3). The very measurements are carried out during periods of 0.2 s when the positive and negative values of the applied axial and transversal field are stabilized. This procedure has been chosen to ensure a high constancy of the applied field during the measurement. Taken all together, the present configuration allows an online monitoring with a time resolution of 6 s.

The most essential problem of the method is the reliable determination of comparably small induced magnetic fields against the background of much higher imposed magnetic fields. Although the magnetic Reynolds number of the flow is of the order of 10^{-1}, the measurable induced fields are typically of the order of 10^{-3}–10^{-2} times the applied field (this has mainly to do with the steep decay of the induced field in the exterior of the fluid.) In order to achieve this objective, an accurate control of the external magnetic field is necessary. By the above mentioned means, the current drift in the Helmholtz coils is controlled with an accuracy of 0.1 %. The temperature drift of the Hall sensor's sensitivity can be overcome by enforcing the applied current to be constant. The temperature drift of the Hall sensor's offset is circumvented by changing the sign of the applied magnetic field (cf. Fig. 3).

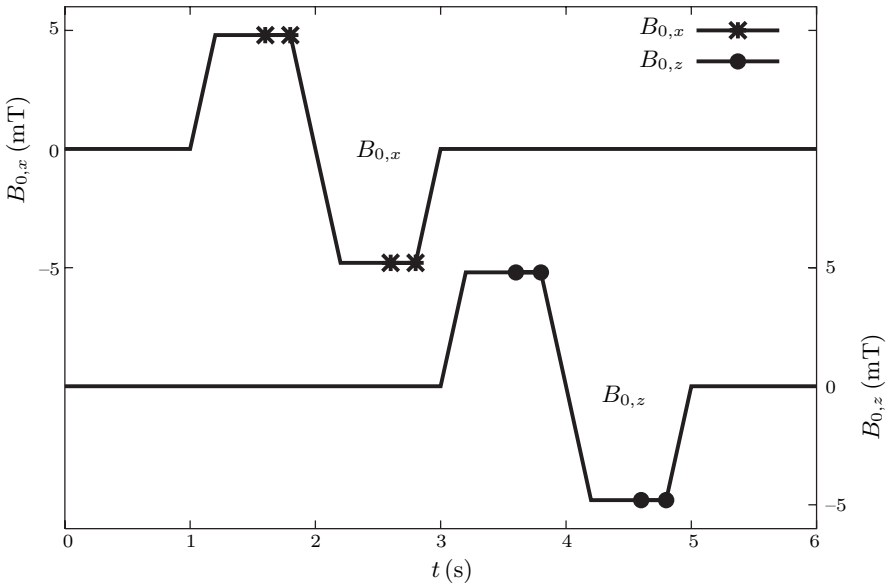

Fig. 3. Sequence in applying the transversal ($B_{0,x}$) and the axial ($B_{0,z}$) magnetic fields. The induced fields are measured in the periods between the crosses and the full circles.

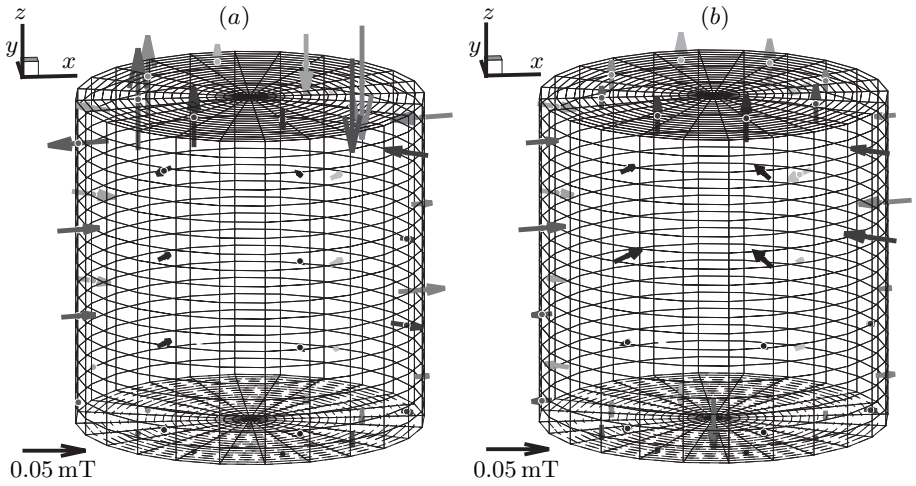

Fig. 4. Measured induced magnetic field components for (a) transverse and (b) axial applied magnetic field. The propeller pumps *upwards* with 1200 rpm. The length of the arrows is proportional to the measured field component, the grey scale indicates the distance from the eye.

For the case when the propeller pumps upwards, Fig. 4a and Fig. 4b exhibit the induced magnetic fields measured at 49 positions for the applied transversal ($B_{0,x}$) and the axial ($B_{0,z}$) field, respectively. From both of these together measured fields, the velocity can be reconstructed.

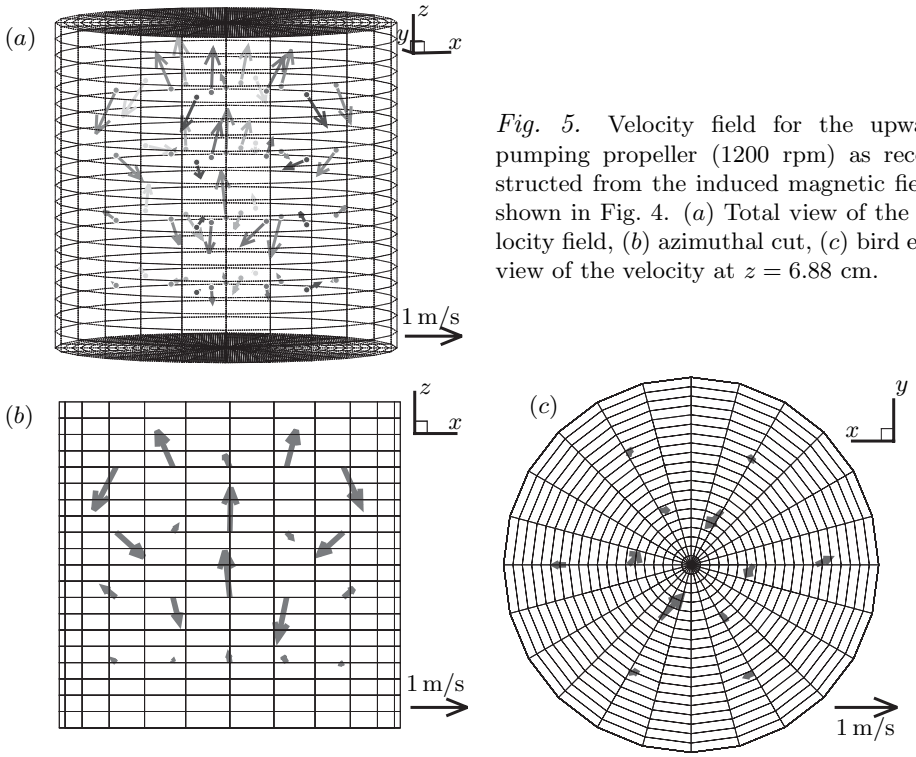

Fig. 5. Velocity field for the upward pumping propeller (1200 rpm) as reconstructed from the induced magnetic fields shown in Fig. 4. (a) Total view of the velocity field, (b) azimuthal cut, (c) bird eye-view of the velocity at $z = 6.88$ cm.

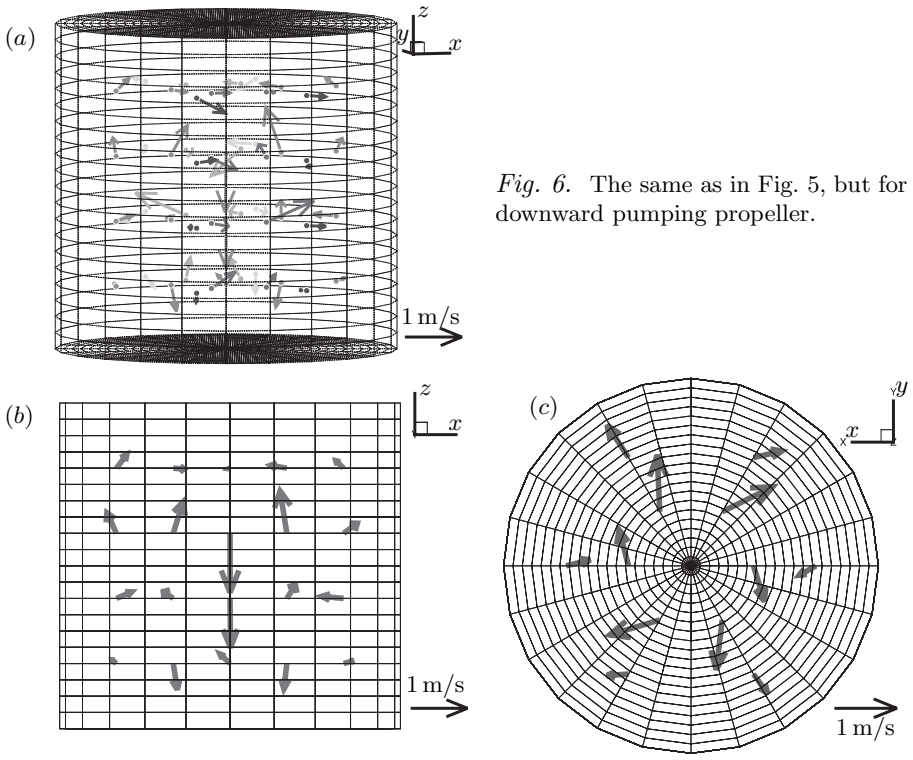

Fig. 6. The same as in Fig. 5, but for the downward pumping propeller.

Figs. 5 and 6 display the results of this inversion for the upward and downward pumping propeller, respectively. For upward pumping, Fig. 5*b* clearly demonstrates an upward flow in the center of the volume and a downward flow at the rim, at least in the upper part of the vessel. In the lower part, the poloidal flow pattern is less pronounced and indicates a possible recirculation zone. Fig. 5*c* shows that there is no significant toroidal flow, which is of course due to the presence of the guiding blades above the propeller.

For downward pumping, the flow pattern is illustrated in Fig. 6. In Fig. 6*c*, we can now identify clearly the rotation of the flow, and in Fig. 6*b* the downward flow in the center and the upward flow close to the rim of the vessel.

In order to validate the CIFT method, we have performed independent velocity measurements based on Ultrasonic Doppler Velocimetry (UDV). Fig. 7 shows the UDV measured axial velocity, at a radius of 8 cm, for four different rotation rates of the propeller, compared to the results of CIFT for a propeller rotation rate of 1200 rpm. While the UDV velocity profiles show basically a scaling behaviour for the propeller rotation rates 300, 500, and 750 rpm, for 1200 rpm there is an apparent problem at larger distances from the ultrasonic transducer. The CIFT reconstruction is shown at four internal points, which are connected by cubic spline interpolation. Evidently, the CIFT is capable of determining the shape and the amplitude of this profile in a reasonable manner. Both techniques reveal a remarkable asymmetry of the flow, with higher values of the axial velocity at the upper part of the vessel and some indication of a recirculating flow (slightly positive v_z) in the lower part. Further comparisons of the measured axial and azimuthal velocities can be found in [2]. Basically, the comparison with UDV measurements shows that the CIFT provides correct and robust results on the main pattern and on the amplitude of the velocity field.

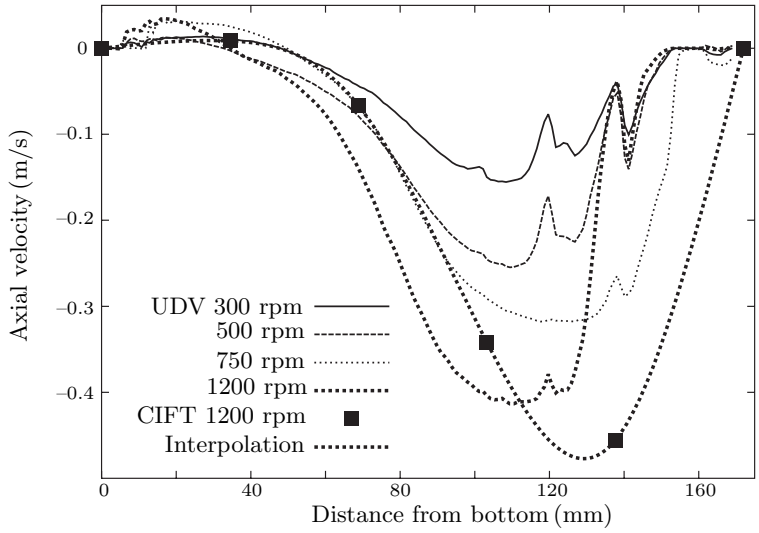

Fig. 7. Comparison of the UDV measured axial velocity component at $r = 8$ cm and the corresponding CIFT values for the upward pumping propeller. The UDV values beyond a distance of 120 mm from bottom are not very reliable for 1200 rpm. The interpolation of the CIFT values is done by a cubic spline approximation.

3. Conclusion. We have demonstrated the feasibility of contactless inductive flow tomography (CIFT) by using the minimal configuration with two orthogonal applied magnetic fields. Presently, the CIFT allows for a transient resolution of the *full three-dimensional flow structure* in steps of a few seconds. This enables an online monitoring of slowly changing flow fields in various processes.

In the presented set-up, the externally applied magnetic field is weak and has no significant influence on the flow to be measured. However, CIFT works as well in cases, where stronger magnetic fields are already present for the purpose of flow control, as, e.g., the electromagnetic brake in steel casting or the DC-field components in silicon crystal growth.

We have also considered the possibility of avoiding the second Helmholtz coil pair, which may be inconvenient for several technological applications. The idea comes to replace the transversal magnetic field by a *cusp field*, which could be produced by the same coil pair as an axial field. Unfortunately, it turns out that the axisymmetric toroidal flow component remains hidden for the cusp field, too.

Obviously, the future of the method lays with replacing the DC fields by the AC fields with different frequencies in order to improve the depth resolution of the velocity field. Roughly speaking, information from different depth layers can be "peeled off" by using fields with different skin depths δ, which depends on the frequency f via $\delta = \sqrt{1/\pi\mu\sigma f}$. Another benefit of using the AC fields is that lock-in techniques can be utilized, which would make the method less sensitive to electromagnetic noise. The integral equation formulation, which can be used for such AC problems has been developed in [9].

Another direction is the generalization of the method to the dynamo relevant regime of high Rm. We can only note here that inference of flow fields from measured magnetic fields has a long tradition in geodynamo theory [10]. First attempts have also been made to use a modified form of CIFT to reconstruct certain flow features of the Riga dynamo experiment [11].

Acknowledgements Financial support from German "Deutsche Forschungsgemeinschaft" under Grant No.GE 682/10-1,2 and in the framework of SFB 609 is gratefully acknowledged.

REFERENCES

[1] M. Hämäläinen, R. Hari, R.J. Ilmoniemi, J. Knuutila, O.V. Lounasmaa. Magnetoencephalography – theory, instrumentation, and application to noninvasive studies of the working human brain. *Rev. Mod. Phys.*, vol. 65 (1993), pp. 413–497.

[2] F. Stefani, T. Gundrum, G. Gerbeth. Contactless inductive flow tomography. *Phys. Rev. E*, vol. 70 (2004), Art. No. 056306.

[3] F. Stefani, G. Gerbeth. Velocity reconstruction in conducting fluids from magnetic field and electric potential measurements. *Inverse Problems*, vol. 15 (1999), pp. 771–786.

[4] J.A. Shercliff. *The Theory of Electromagnetic Flow-Measurement* (Cambridge University, Cambridge, 1987).

[5] M. Xu, F. Stefani, G. Gerbeth. The integral equation method for a steady kinematic dynamo problem. *J. Comp. Phys.*, vol. 196 (2004), pp. 102–125.

[6] F. Stefani, G. Gerbeth. On the uniqueness of velocity reconstruction in conducting fluids from measurements of induced electromagnetic fields. *Inverse Probl.*, vol. 16 (2000), pp. 1–9.

[7] F. Stefani, G. Gerbeth. A contactless method for velocity reconstruction in electrically conducting fluids. *Meas. Sci. Technol.*, vol. 11 (2000), pp. 758–765.

[8] F. Stefani, G. Gerbeth, Th. Gundrum. A contactless inductive velocity reconstruction method for metallic and semiconducting melts. *Mater. Manuf. Process.*, vol. 19 (2004), pp. 651–663.

[9] M. Xu, F. Stefani, G. Gerbeth. Integral equation approach to time-dependent kinematic dynamos in finite domains. *Phys. Rev. E*, vol. 70 (2004), Art. No. 056305.

[10] P.H. Roberts, S. Scott. On the analysis of secular variation. 1. A hydromagnetic constraint - Theory. *J. Geomag. Geoelectr.*, vol. 17 (1965), pp. 137–151.

[11] F. Stefani, A. Gailitis, G. Gerbeth, Th. Gundrum, M. Xu. Forward and inverse problems in MHD: numerical and experimental results. *GAMM Mitteilungen*, in press (2006).

Received 03.04.2006